ROLE OF WESTERN BOUNDARY CONDITIONS IN ENSO EVENTS SIMULATED BY A COUPLED OCEAN-ATMOSPHERE MODEL OF THE TROPICAL PACIFIC

by

Pierre Florenchie (*), Claire Perigaud and Jean-Philippe Boulanger

in preparation for *Satellites, Oceanography and Society*

edited by D. Halpern, Elsevier, New York.

April 30th, 1999.

Pierre Florenchie and Claire Perigaud, Jet Propulsion Laboratory, California Institute of Technology, MS 300/323, 4800 Oak Grove Dr., Pasadena, CA 91109, USA.

Jean-Philippe Boulanger, Laboratoire d'Oceanographie DYnamique et de Climatologie, CNRS-Universite Pierre et Marie Curie, Boite Postale 100, 4 Place Jussieu, 75252 Paris cedex 05, France.

(*) to whom correspondence should be addressed:

phone= 818 354 0881, fax= 818 393 6720, email=flp@pacific.jpl.nasa.gov

Abstract

This study examines the role of the Indonesian Throughflow (ITF) variations on the ElNiño/LaNiña events simulated by a coupled ocean-atmosphere model of the tropical Pacific. Two sea level data sets are used to estimate ITF transport interannual variations over 1980-1998. It is found that the transport generally decreases during El Niño events and increases during La Niña events. The Pacific ocean model has been used either forced by observed wind stress, or coupled with a statistical atmosphere. In each case, two different configurations of the western boundary are investigated, one with a closed western boundary and the other with a prescribed ITF. When the western boundary is closed, the model used in a forced mode shows good skill in reproducing warm and cold events in terms of sea surface temperature, sea level and wind anomalies. No major differences are found when the ITF is prescribed at the western boundary. But when the model is used in a coupled mode, the prescription of the ITF has a very strong impact on the forecasts.

I - Introduction

The Indonesian Throughflow (ITF) is supposed to have considerable implications on the global climate. It connects dynamically and thermodynamically the Indian and Pacific oceans on different time scales, via three major passages: the Lombok strait, the Savu strait and the Timor strait. It has also been suggested as the major return flow of thermocline water from the Pacific ocean to the Atlantic ocean (Gordon and Piola, 1983; Gordon 1985; Gordon, 1986). Many authors, like Toole

(1987) or Kindle and al. (1989) claim that the accurate determination of the heat, mass and salt fluxes in the Pacific and Indian oceans requires an accurate knowledge of the ITF. But, as noted by Godfrey (1996), the ITF magnitude and its variability are still poorly known. Substantial differences appear in transport estimates inferred from observations or modelling experiments. Mean transport values range from 5 to 16 Sv from the Pacific ocean to the Indian ocean. The ITF variability shows a strong seasonal signal, with smaller amplitude in boreal winter and larger one in summer.

Attention has also turned to the Indonesian Throughflow because of its possible connection with large scale phenomena such as ENSO events. Interannual variations of the ITF transport have been observed in different studies. They seem to be related with ENSO events occurring in the tropical Pacific. The ITF transport from the Pacific to the Indian ocean is weaker during El Niño and stronger during La Niña (Clarke and Liu, 1994; Vershell et al., 1995; Meyers, 1996; Murtugudde et al., 1998). In general, the ITF tends to warm the eastern Indian ocean and cool the western Pacific warm pool. Therefore, its variations are likely to have a strong effect on the variability of the coupled ocean-atmosphere system, including remote areas such as the cold tongue. Most of its interannual variability seems to be controlled by interannual wind anomalies over the Pacific ocean (Murtugudde et al., 1998).

The goal of this study is to investigate the impact of the ITF on simulations and forecasts of ENSO events. Experiments are carried out using a model of the

tropical Pacific ocean coupled to a statistical atmosphere, such as in Boulanger (1999). The model is either forced by CAC (Climate Analysis Center) SST data via the statistical atmosphere or free to evolve in a forecast mode. In each case, two different configurations of the western boundary are investigated: either it is closed, or values of inflow/outflow derived from observations are prescribed at the western boundary, in an attempt to investigate the impact of the ITF anomalies on the ENSO events.

In the next section, we describe the data used in this study to build the time series of the interannual variations of the ITF over 1980-1998. In the third section, we present the control run during which the ocean model is forced by the statistical atmosphere with its western boundary closed. The fourth section is dedicated to the calculation of the ITF and its analysis. In section 5, results of the forced mode experiments are presented. In the sixth section, we discuss preliminary results of the coupled model experiments. Finally, section 7 gives some perspectives.

II - The Data

Monthly sea level anomalies (SLA) over the Indian and Pacific oceans were derived from eXpandable BathyThermograph sondes (XBT) between January 1980 and March 1998 and from the altimetric variations derived from the satellite TOPEX/Poseidon (TP) between October 1992 and June 1998. Hydrographic data actually do not provide sea level, but different quantities can be computed as a proxy

to sea level. Our estimates are derived from the analyzed fields provided by Dr. Smith from Bureau of Meteorology Research Center since January 1980 with regular updtates (Smith et al., 1995). We use here the vertical temperature profiles to estimate the dynamic height (hdyn) at the surface relative to 400m. The two monthly fields are initially interpolated on a 1° by 1° grid.

Monthly varying climatologies have been computed over January 1980-December 1996 for hdyn, and over January 1993-December 1996 for TP to determine the anomalies. Then, a reference surface has been added to the TP anomalies, because altimeters provide variations of sea level relative to its average over the satellite period. Hdyn anomalies are relative to a longer period, and are not negligible on average over the short satellite period. Hence, TP anomalies are corrected with the mean hdyn anomalous surface calculated from October 92 to March 98 over the Indian and Pacific oceans (see Figure 1.a). In the Pacific ocean, significantly positive values ranging from 2 to about 4 cm are observed between 160°E and 110°W, mainly between the equator and 10°S, while negative values with similarly large amplitude occur in the western Pacific, between the equator and 20°N. In the Indian ocean, the reference surface shows a zonal tilt with weaker amplitudes of about +1cm in the west and -1cm in the east. Thus negative values occur in the Indo-Pacific area, while positive values take place on the opposite side of each ocean. This reference surface corresponds to changes of the ocean in the early 1990s which had the opposite sign during the previous twelve years. It reveals possible large-scale mass exchanges between the two oceans. It is striking that it

indicates heat content deficit over the Indo-Pacific warm pool and excess over the cold tongues of the Pacific and Indian oceans, with the largest values in the Pacific ocean. Note here that it is crucial to add the correct reference surface to TP anomalies before using these data to initialize a forecast model (see, Perigaud et al.; 1999).

TP satellite provides actual sea level variations. In addition, they are more accurate than hdyn anomalies which do not account for salinity variations and are referenced to a fixed level at depth. The RMS variability fields of each data set over the satellite period were compared and their ratio (fig. 1b) determines the multiplifying coefficient to be applied to hdyn anomalies in order to get the same variability at each point during the satellite period. It appears that hdyn fit TP quite well over the equatorial Pacific ocean between 10°S and 10°N, with values ranging from 0.75 to 1.25. As anticipated, important corrections are necessary north of 10°N and south of 10°S, with a correction factor superior to 2 in some areas. The ratio is larger in the Indian ocean: hdyn underestimates significantly the variability of sea level over most of the basin.

It is worth noting that in both oceans, the eastern part of the basins has large ratios, with values greater than 2. It is likely that this is not only due to the fixed 400m reference, nor to the lack of salinity in hdyn which is crucial in the western Pacific as much as in the eastern Indian Ocean. The underestimation is possibly due to the poor coverage of the in-situ data. In addition, in the south Indian ocean, a

deeper reference level would be more adequate to account for the full variability associated with the ITF (Broecker, 1991).

Figure 2 highlights the impact of the corrections applied on hdyn and TP. Compared to figures 2.ab, figures 2.cd show clearly that despite unavoidable differences between the data sets, the two estimates agree reasonably well. In the rest of the paper, hdyn is used from January 1980 until September 92, and TP data from October 1992 to June 1998 in a continuous time series.

III - The model and the control run

The model used in this study is a coupled ocean-atmosphere intermediate model. The ocean model is the TRIDENT model. Its complete description and validation over the TP period can be found in Boulanger (1999). This ocean model is a reduced-gravity anomaly model with Ekman shear and mixed thermodynamic layer at the surface. The climatological fields derived from data are prescribed into the mixed layer. The domain extends from 130°E to 98°W, and from 20.25°S to 20.25°N, and has a landmask. The horizontal resolution is 2° in longitude, and 0.5° in latitude. The atmospheric model is a statistical one, based on bilinear regression between the CAC surface temperature and the FSU (Florida State University) wind pseudo-stress anomaly observations, similar to the one used in Cassou and Perigaud (1999).

The first experiment (control run) consists in simulating the 1980-1998 ENSO events using the model with a closed western boundary and forced by observed sea surface temperature anomalies (SSTA) from January 1980 to June 1998. Model outputs are monthly averaged.

Figures 3 and 4 display maps of variability inferred from model outputs or observations. It is worth noting here that in Boulanger (1999), the model is forced by ERS+TAO winds stress data during the 92-98 period, and validated versus TP data. In the present study, the model is forced by CAC SSTA from January 80 to June 98. Figures 3.a and 4.a show the simulated and observed sea level variability over the simulation period. Main patterns of observed variability occur along the equator east of the dateline with amplitudes higher than 8cm, and in the off-equatorial areas: between 160°E and 170°W south of the equator (maximum of about 8cm), between 130° and 160°E north of the equator (amplitudes higher than 7cm). The simulated sea level shows weaker variability along the equator with maximum amplitudes below 7cm. The western pattern south of the equator is reproduced with higher amplitudes (about 12cm) while north of the equator, the simulated sea level variability shows weaker amplitudes west of 145°E. Its maximum is centered near 170°E, east of the observed one.

Figures 3.b and 4.b display the simulated and observed sea surface temperature variability from January 1980 to June 1998. The two figures show strong similarities. The model reproduces the correct main patterns of variability, mostly

located in the equatorial eastern Pacific. The model reproduces the observed double-peak SST pattern, one offshore located slighted south of the equator, with a maximum of about 1.3°C at 120°W, and the strongest well-known coastal maximum along Peru, with an amplitude of about 1.8°C (fig. 3b). Indeed, the model reproduces the observed amplitudes fairly well (fig. 4b).

Figures 3.c and 4.c represent the zonal wind stress variability calculated from simulated and observed sea surface temperature anomalies via the statistical atmosphere. The main patterns are correctly reproduced, with highest amplitudes centered on the equator between 170°E and 120°W, and between 10°S and 5°N. Maxima of variability occur between the dateline and 160°W slightly south of the equator on both figures, but with weaker values for the model than for the data (0.18 dyn/cm^2 versus 0.24 dyn/cm^2).

Figures 3.d and 4.d represent the meridional wind stress variability calculated from simulated and observed sea surface temperature anomalies via the statistical atmosphere. Main patterns of variability are realistically simulated, with highest values between 180°E and 110°W, north of the equator and south of 10°N. A maximum takes place near 140°W and 5°N on both figures, with slightly stronger values for the model than for the data (0.20 dyn/cm^2 versus 0.18 dyn/cm^2). Note that a similar coupled model with a different statistical decomposition, a different ocean model and different data sets, also gives too weak an amplitude for the zonal

stress and too strong for the meridional stress (Cassou and Perigaud, 1999). Slightly modulating the drag coefficient allows to partly address this deficiency.

In summary, the model shows good skills in reproducing the sea surface temperature variability when it is forced by observed SSTA, with a closed western boundary. As a consequence, the inferred wind variability calculated from the SSTA outputs via the statistical atmosphere shows strong similarities with the one calculated directly from CAC data and used to force the ocean model. Some differences occur between the observed sea level variability and the simulated one. Similar deficiencies were found in Cassou et Perigaud (1999). In the western region, one possible explanation is that the condition of reflection of Rossby waves into the equatorial Kelvin waves is not fully verified in reality. Indeed, TP data and ERS data indicate that full reflection does not always take place (Boulanger and Fu, 1998).

IV - An estimate of the Indonesian Throughflow interannual variations

We make here the assumption that the differences between the observed and the simulated SLA occuring close to the western boundary of the model can be accounted for by the Indonesian Throughflow. It is certainly not the only source of discrepancy in the sea level over the western Pacific. Neglecting salinity or using wind data that are inaccurate are also major concerns. Nevertheless, this is an assumption which is of great interest here, as the wind and the wave full reflection explain a large part of the observed variability in the western tropical Pacific ocean,

and as the ocean model is known to well represent this type of dynamic. In addition, the TRIDENT model used here separates the Kelvin and Rossby components of sea level, and writes explicitely the full reflection of Rossby waves by summing up all the corresponding geostrophic zonal current anomalies to determine the Kelvin amplitude at the western boundary. So it is appriopriate to study the ITF impact by modulating the amplitude of the Kelvin component at this boundary.

First, the observed SLA have been interpolated onto the model grid. Then, geostrophic velocity time series have been calculated using either the observed or the simulated sea level fields, from January 1980 to June 1998 (figure 5.a), following the method described in Delcroix at al. (1994). We have verified with the control run outputs that this method works well to deliver the correct velocity estimates. Then, the difference between the simulated geostrophic velocity fields and the ones derived from observations is calculated at each point, from Junuary 80 to June 98. The integration of the difference between 2.25°N and 7.25°N (11 grid points) at 134°E is considered as due to the ITF (figure 5.b). The longitude 134°E is chosen because west of it, SL observations are close to coast lines and provide less accurate geostrophic current estimates. The choice of the latitudes 2.25°N and 7.25°N correspond to the opening in the western Pacific where the ITF first enters the Indonesian region. During model integrations that take into account the oceanic connection between the Pacific and the Indian oceans, ITF velocity values are added to the Rossby currents at these latitudes to determine the Kelvin amplitude at the western boundary.

On both figures, assuming that the transport is 100 meters deep with a uniform speed on the verticale, a velocity of 10 cm/s corresponds to a transport anomaly of about 5 Sverdrup eastward. Our estimate of the ITF interannual variability is in good agreement with many other studies (see section 1). The ITF interannual variability shows a signal strongly related to ENSO, with a transport increase to the Indian ocean during the cold events of 1984/85, 1988/89, and a decrease during warm events: minima arise in 1982/83, 1986/87, 1991, and 1997. We also note on figure 5.b a decadal trend with a tendency to decreasing transport. After a westard maximum transport in 1992, years from 1993 until 1997 are dominated by a continuous eastward transport anomaly.

V - Forced simulations with a prescribed ITF at the western boundary

In this section, the time series of ITF geostrophic velocity anomalies is prescribed at the western boundary of the model, as explained above. It is worth noting here that the ocean model does not conserve mass because of the long wave approximation. We prescribe anomalies which correspond to inflow or outflow at the western boundary without further modifications in the model, their 17-year mean being zero by definition. Except for the western boundary condition, the configuration of the model is identical to the control run one. Results are compared to the control run outputs on figures 6.a, 6.b and 6.c.

First, note on each figure that the ITF prescription does not modify very significantly the results of the forced simulations. It slightly changes both the amplitude of anomalies and the phase of the events. Figure 6.a shows that the deficiency of the model is slightly reduced from 1986 to 1988, and from 1994 to 1996. In 1983, the model is not much affected. The negative SLA amplitude are too strong whether the ITF is applied or not. Similar deficiency was found for a different model and is interpreted as being partly due to the poor data coverage at that time (Perigaud et al., 1999). The forced model shows better skills in reproducing SSTA over the 80-98 period (figure 6.b). The prescription of the ITF improves the behaviour of the model in 1985, in 1990, and during the peaks of the 82/83 and 97/98 events. It has a weak impact during the decline of each warm event and during the years 1980/1981, 1989, 1990, and 1992/93. It has a negative impact in 1982, 1987, 1991/92, 1994 and from 1995 to 1997: with a prescribed ITF, the model shows a tendency to be warmer than observations by about 0.5°C. For the wind, differences between the two configurations are not significant. Note that during the onset the warm events, the weakening of the trade winds is simulated by about one month earlier with the ITF than without.

Athough the prescription of the ITF does not modify drastically the results of the model during forced simulations, it is anticipated that weak differences, especially during the onset of the warm events, will have very big impacts on coupled simulations because of the positive feedbacks between the ocean and the atmosphere. Figures 7 highlights the ITF effects between the two forced simulations

when sea level anomalies are averaged over the whole basin, between 5°S and 5°N, from 130°E to 80°W. Significant differences arise both in amplitude and phase, during all the period. From 1980 to 1987, and then in 1989, the deficiency of the model is clearly reduced, while the opposite is found in 1987, and from 1994 to 1996. The sea level averaged over the whole basin is a good indicator of the heat content of the ocean which plays a key role in the interaction between the ocean and the atmosphere (Cassou and Perigaud, 1999). Hence, let us examine the impact of prescribing the ITF on forecasts.

VI - Impact of the ITF on coupled simulations

Series of two-year long forecasts have been carried out with either a closed western boundary, or a prescribed ITF. For the two configurations, identical initial conditions (provided by the control run) are used to start the simulations. Past these conditions, the ocean model is no longer forced by observed SSTA, but by its own SSTA outputs, turned into pseudo-wind stress via the statistical atmosphere at each time step. Results are presented for the 1981-1986 period in figure 8.

The behavior of the coupled model is mainly modified before the growing phase of the warm 82/83 event: without the ITF, the coupled model is not able to reproduce the growing of the warm event before initial SST conditions are warm enough (June 1981 to November 1981). With the prescription of the ITF, the coupled model is successful to predict the onset of the warm event, although with a delay of

a few months for the first four forecasts. The delay disappears with the fifth forecast initialized in January 82, when the SSTA starts being positive. Afterwards, the coupled model shows similar ability with and without the prescribed ITF until January 1983. Then during the decay of the warm event, differences occur again: the coupled model with the closed western boundary predicts a second warming while with the prescribed ITF, the coupled model continues to predict the observed decay of the warm event. The latter is consistent with the evolution of the ITF becoming negative. A positive ITF anomaly helps the growing of the warm event, while a negative value helps its decay, but this relation is far from being linear. In particular, the impact of ITF during the growing phase of the first forecasts on figure 8.b is considerably larger than during any other time. This is because the ITF helps to trigger the minimal SSTA warming above which the coupled model enters in a growing warm event.

VII - Conclusions

The impact of the Indo-Pacific connection on ENSO over the tropical Pacific has been investigated using estimates of interannual ITF variations from January 1980 to June 1998 and an ocean-atmosphere model of the tropical Pacific. First, a strong correlation appears between the occurrence of observed ENSO events in the tropical Pacific and ITF interannual variations: during warm events, the ITF westward transport decreases while during cold events, it increases. Observed SSTA Niño3 index indicates that each ENSO event is associated with similar ITF

variations, but with some modulations in the amplitude and the phase. During simulations of the 82/83 ENSO event, the prescription of the ITF modifies drastically the results of the coupled model. Given the extreme sensitivity of coupled model, such an impact is not surprising. But it was not expected that the skill of the coupled model would be so significantly improved: the prescription of the ITF at the western boundary has a very strong and positive effect on the simulations of SSTA in this case. The sole modification of the reflection of Rossby waves at the western boundary allows to trigger the warm event. This experiment highlights the importance of the Indo-Pacific connection for ENSO simulated by the model. Our results also show that each ENSO event is unique, and the ITF role may not be the same from one event to the other. Nevertheless, these preliminary results suggest that a positive ITF anomaly helps the model to trigger a warm event, while a westward anomaly enhances a reversal of the warm event. In future papers, we will explain in detail the impact of the ITF duringthe forecasts of ENSO events from 1980 to 1998, or the during 19 year-long coupled simulations.

Acknowledgments

The research described in this paper was carried out by the Jet Propulsion Laboratory, California Institute of Technology, under a contract with the National Aeronautics and Space Agency.

List of references

Boulanger, J.-P., The Trident Pacific Model, Part 1: The oceanic dynamical model and observations during the TOPEX/POSEIDON period, Submitted to *Climate Dynamics*, Feb. 1999.

Boulanger, J.-P., and C. Menkes, The Trident Pacific Model, Part 2: The thermodynamical model and the role of long equatorial wave reflection during the TOPEX/POSEIDON period, Submitted to *Climate Dynamics*, Feb. 1999.

Boulanger, J.-P., and L. L. Fu, Evidence of boundary reflection of Kelvin wave and first-mode Rossby waves from TOPEX/Poseidon sea level data, *J. Geophys. Res.*, 101, 16361-16371, 1996.

Broecker, W. S., The great ocean conveyor, *Oceanography*, 4, 79-89, 1991.

Cassou, C., and C. Perigaud, ENSO simulated with Intermediate Coupled Models And evaluated with observations over 1970-1998, Part II: Importance of the off-equatorial wind and ocean, *J. Climate*, revised version, 1999.

Clarke, A., and X. Liu, Interannual sea level in the northern and eastern Indian Ocean, *J. Phys. Oceanogr.*, 24, 1224-1235, 1994.

Delcroix, T., J.-P. Boulanger, F. Masia, and C. Menkes, GEOSAT-derived sea level and surface-current anomalies in the equatorial Pacific, during the 1986-1989 El Niño and La Niña, *J. Geophys. Res., 99*, 25093-25107, 1994.

Fieux, M., C. Andrie, P. Delecluse, A. Ilahude, A. Karstavsteff, F. Mantisi, R. Molcard and J. Swallow, Measurements within the Pacific-Indian Oceans throughflow region, *Deep Sea Res., 41*, 1091-1130, 1994.

Fieux, M., R. Molcard and A. Ilahude, Geostrophic transport of the Pacific-Indian Oceans throughflow, *J. Geophys. Res., 101*, 12421-12432, 1996.

Kindle, J., H. Hurlburt, and E. Metzger, On the seasonal and interannual variability of the Pacific to Indian ocean throughflow, paper presented at the Western Pacific *International Meeting and Workshop on TOGA COARE*, ORSTOM, Noumea, New Caledonia, 1989.

Godfrey, J. S., A Sverdrup model of the depth-integrated flow for the world ocean allowing island circulations, *Geophys. Astrophys. Fluid. Dyn., 45*, 89-112, 1989.

Godfrey, J. S., The effect of Indonesian throughflow on ocean circulation and heat exchange with the atmosphere, *J. Geophys. Res., 101*, 12217-12237, 1996.

Gordon, A., and A.R. Piola, Atlantic Ocean upper layer salinity budget, *J. Phys. Oceanogr., 13*, 1293-1300, 1983.

Gordon, A., Indian-Atlantic transfert of thermocline water at the Agulhas Retroflection, *Science, 227*, 1030-1033, 1985.

Gordon, A., Interocean exchange of thermocline water, *J. Geophys. Res., 91*, 5037-5046, 1986.

Hirst A.C., and J.S. Godfrey, The role of Indonesian Throughflow in a global ocean GCM, *J. Phys. Ocean.*, Vol. 23, 1057-1086, 1993.

Lee, T., J.-P. Boulanger, A. Foo, L.L. Fu and R. Giering, Data Assimilation by an intermediate coupled ocean-atmosphere model: application to the 1997-98 El Niño, Submitted to *J. Geophys. Res.*, 1999.

Meyers, G., Variation of Indonesian throughflow and the El Niño Southern Oscillation, *J. Geophys. Res.*, Vol. 101, No C5., 12225-12263, 1996.

Murtugudde, R., A. J. Busalacchi, and J. Beauchamp, Seasonal to interannual effects of the Indonesian throughflow on the tropical Indo-Pacific Basin, *J. Geophys. Res., 103*, 21425-21441, 1998.

Perigaud, C., C. Cassou, B. Dewitte, L.L. Fu, and D.J. Neelin, Use of data to improve Seasonal to Interannual forecasts simulated by Intermediate Coupled Models, Submitted to *Mon. Wea. Rev.*, 1999.

Schneider N., The Indonesian Throughflow and the Global Climate System, *J. Climate*, Vol 11, No.4, 676-689, 1998.

Smith, N. R., An improved system for tropical ocean subsurface temperature analyses, *J. Atmos. Oceanic. Technol., 12*, 850-870, 1995.

Toole, J. M., Problems of interbasin exchanges and marginal-sea overflows, *Bull. Am. Meteorol. Soc., 68*, 136-140, 1987.

Vershell, M., J. Kindle, and J. O'Brien, Effects of Indo-Pacific throughflow on the upper tropical Pacific and Indian Oceans, *J. Geophys. Res., 100*, 18409-18420, 1995.

Wajsowicz, R. C., A relationship between the interannual variations in the south Pacific wind stress curl, the Indonesian throughflow and the west Pacific warm water pool, *J. Phys. Oceanogr., 24*, 2180-2187, 1994.

REFERENCE SURFACE FROM HYDROGRAPHIC DATA - OCT 92-MARCH 98 - UNIT:CM

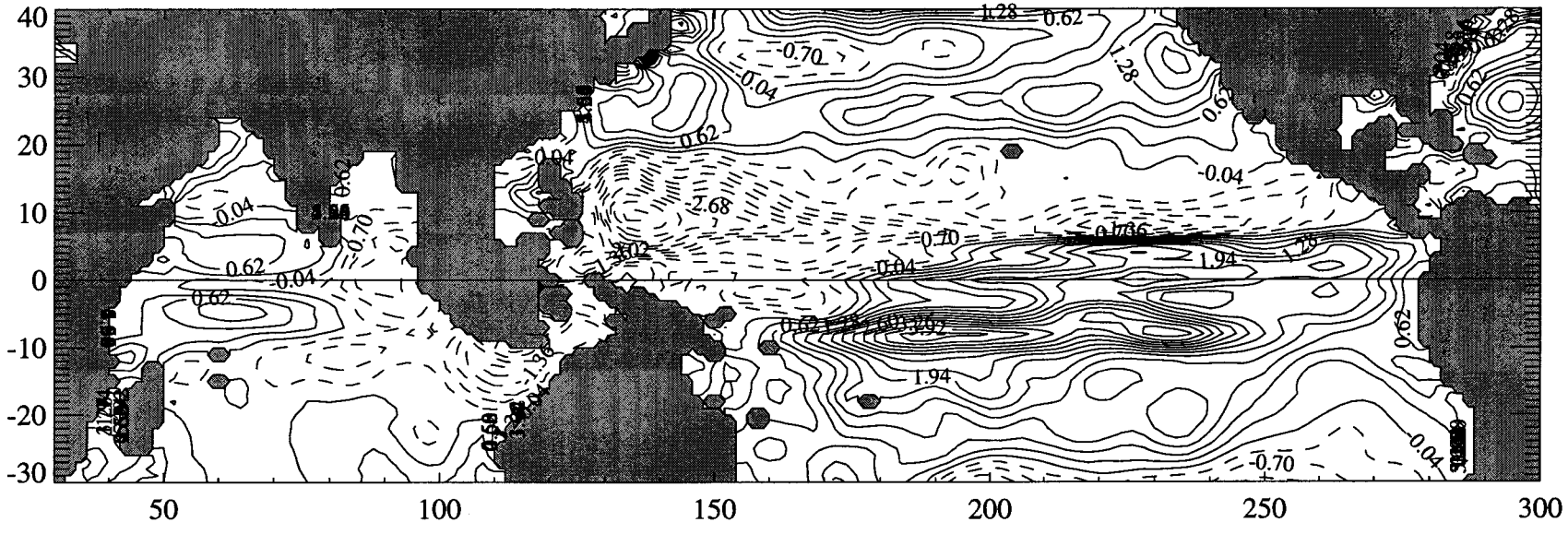

SATELLITE/HYDROGRAPHIC DATA RMS RATIO - OCT 92-MARCH 98

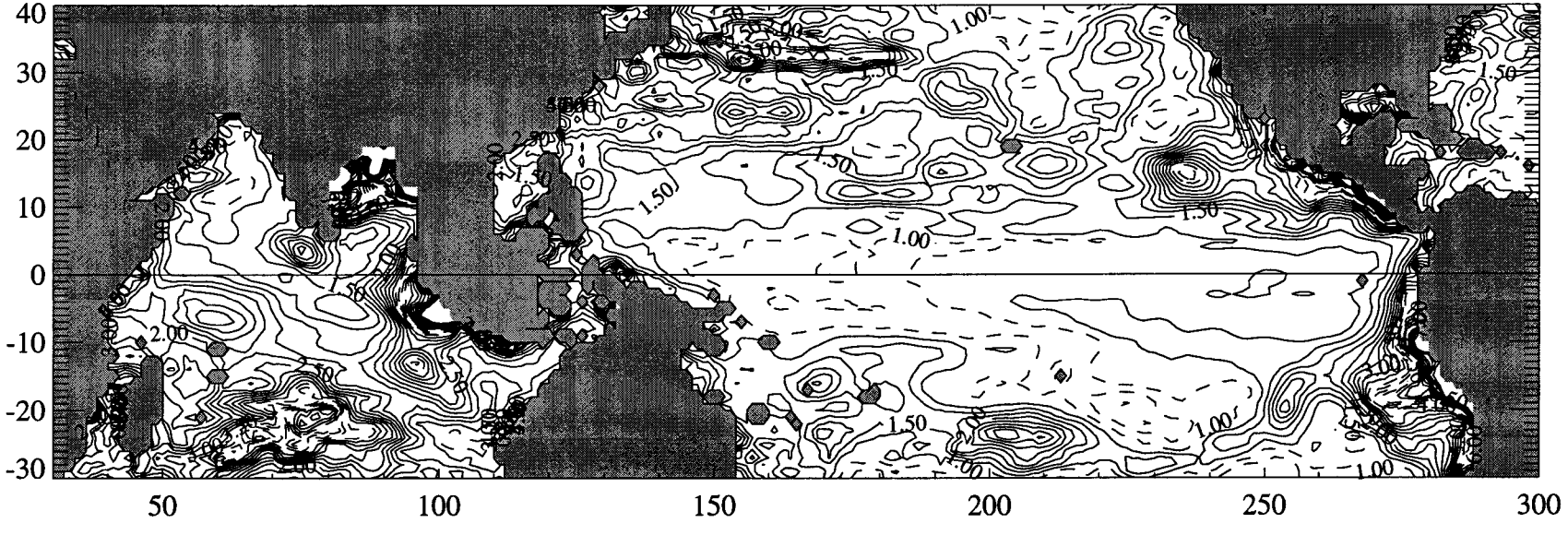

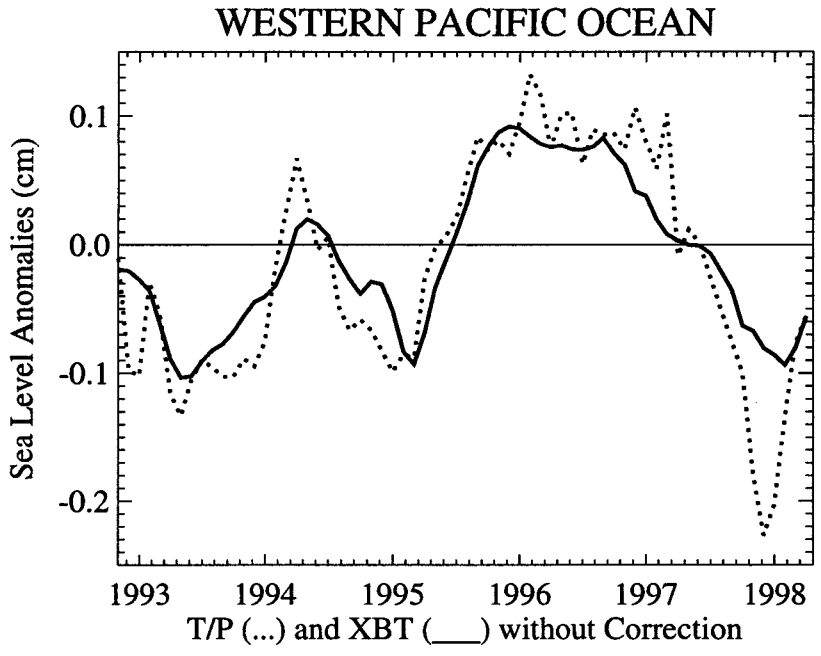
WESTERN PACIFIC OCEAN
Sea Level Anomalies (cm)
0.1
0.0
-0.1
-0.2
1993
1994
1995
1996
1997
1998
T/P (...) and XBT (___) without Correction

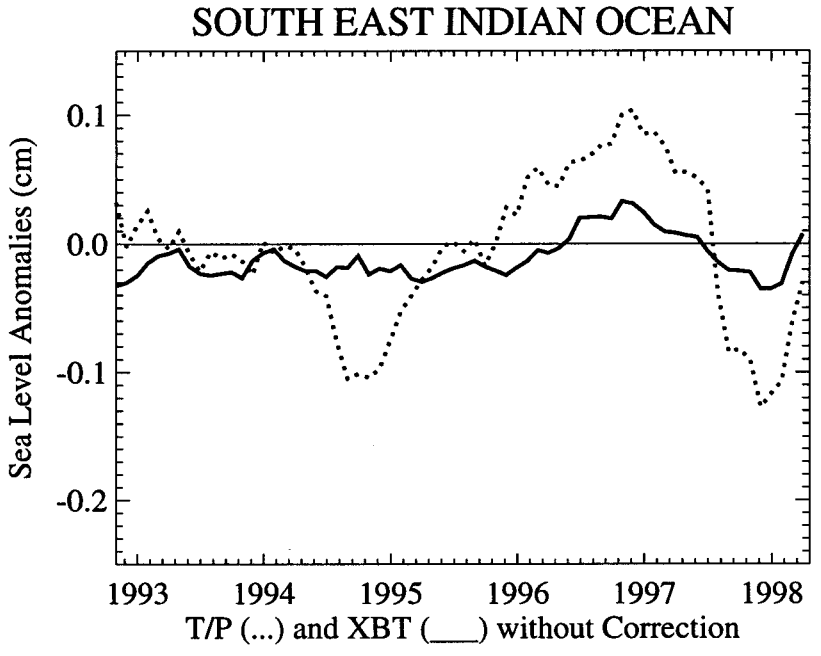
SOUTH EAST INDIAN OCEAN
Sea Level Anomalies (cm)
0.1
0.0
-0.1
-0.2
1993
1994
1995
1996
1997
1998
T/P (...) and XBT (___) without Correction

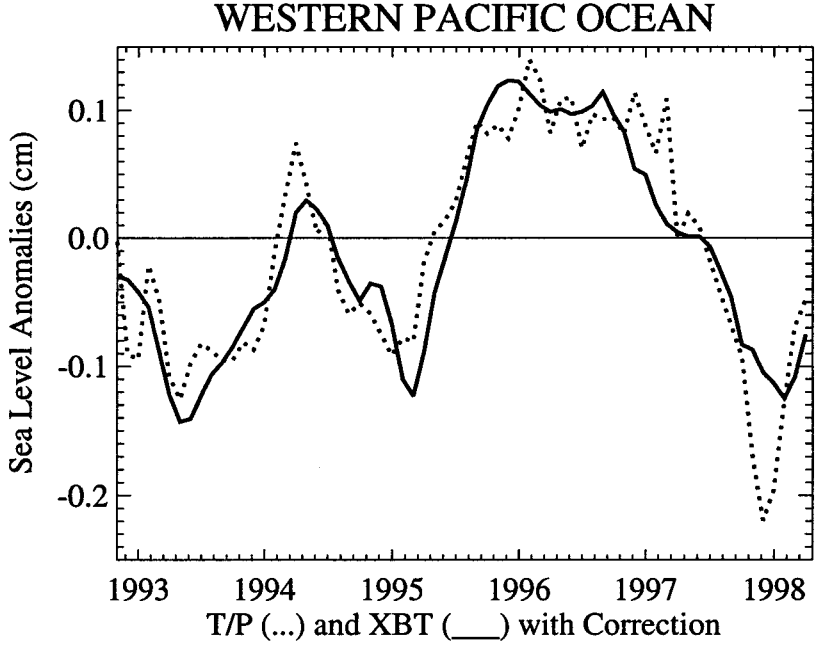
WESTERN PACIFIC OCEAN
Sea Level Anomalies (cm)
0.1
0.0
-0.1
-0.2
1993
1994
1995
1996
1997
1998
T/P (...) and XBT (___) with Correction

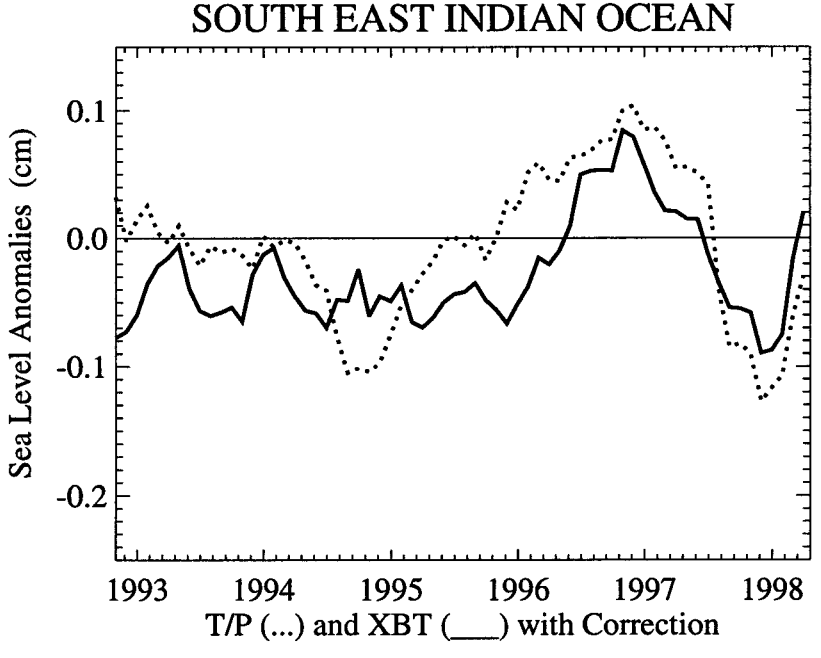
SOUTH EAST INDIAN OCEAN
Sea Level Anomalies (cm)
0.1
0.0
-0.1
-0.2
1993
1994
1995
1996
1997
1998
T/P (...) and XBT (___) with Correction

RMS of OBSERVED SEA LEVEL ANOMALIES (CM) - Hdyn+TP DATA

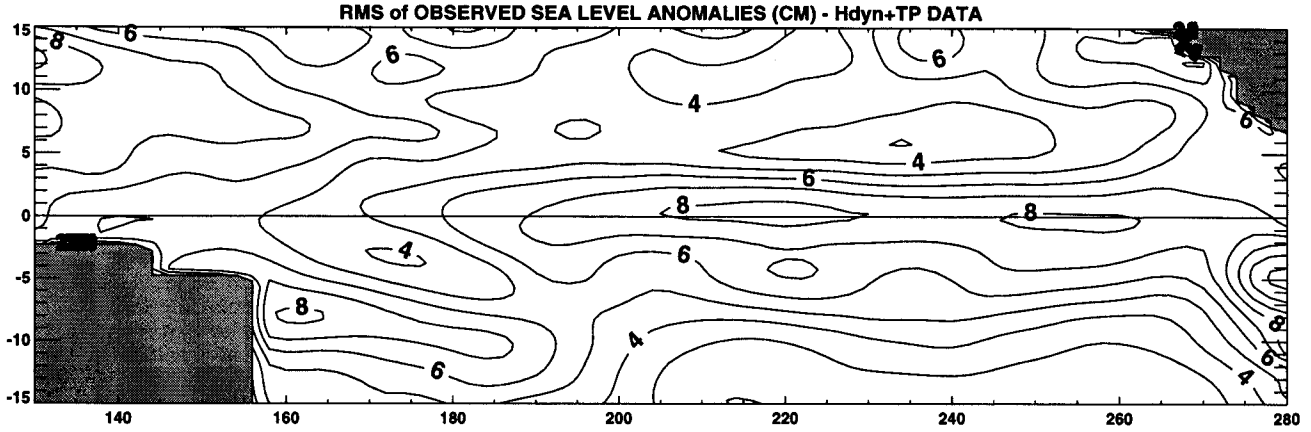

RMS of OBSERVED SST ANOMALIES (C) - CAC DATA

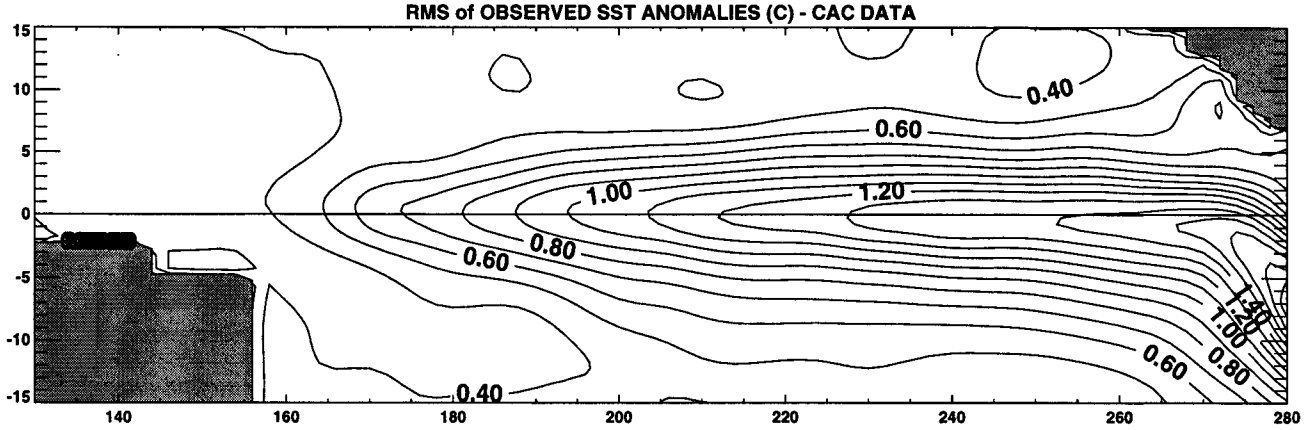

RMS of CAC STAT ZONAL WIND STRESS ANOMALIES (DYN/CM2)

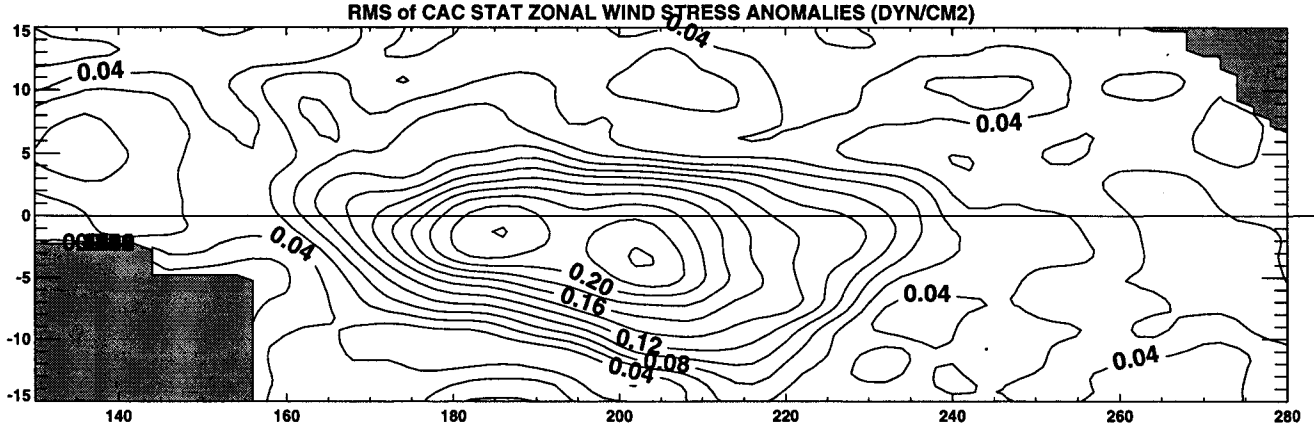

RMS of CAC ASTAT MERIDIONAL WIND STRESS ANOMALIES (DYN/CM2)

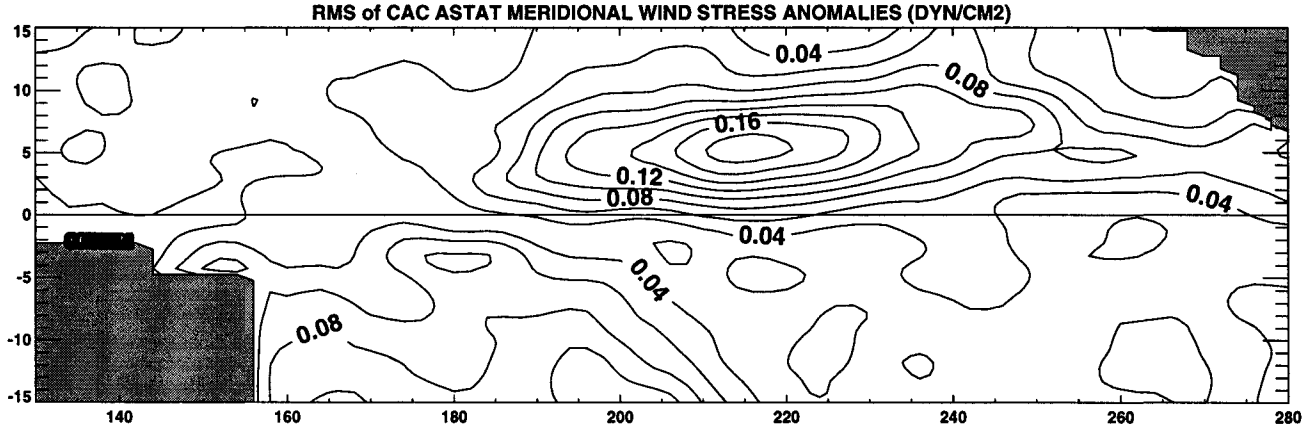

SEA LEVEL ANOMALIES (CM) - CONTROL RUN

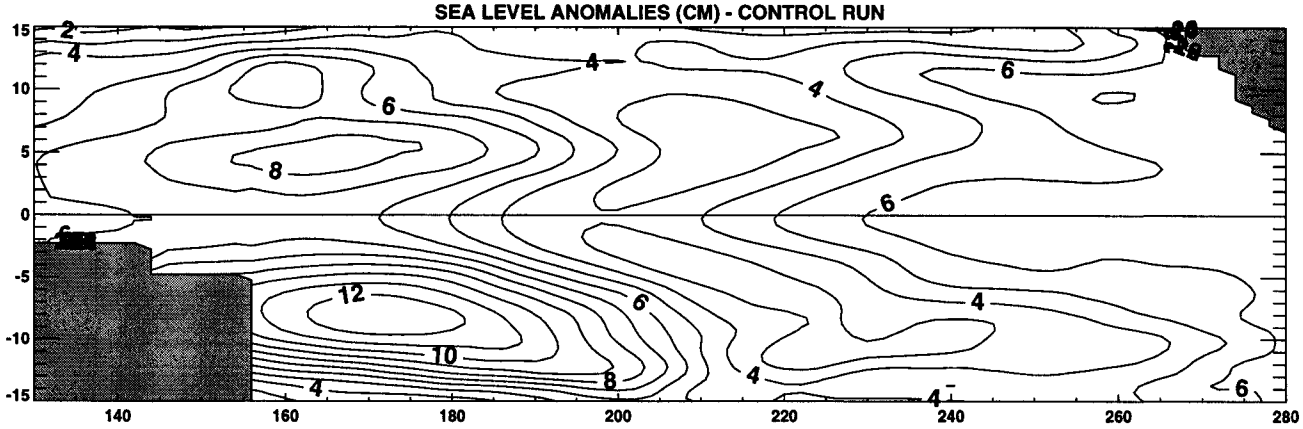

SST ANOMALIES (C) - CONTROL RUN

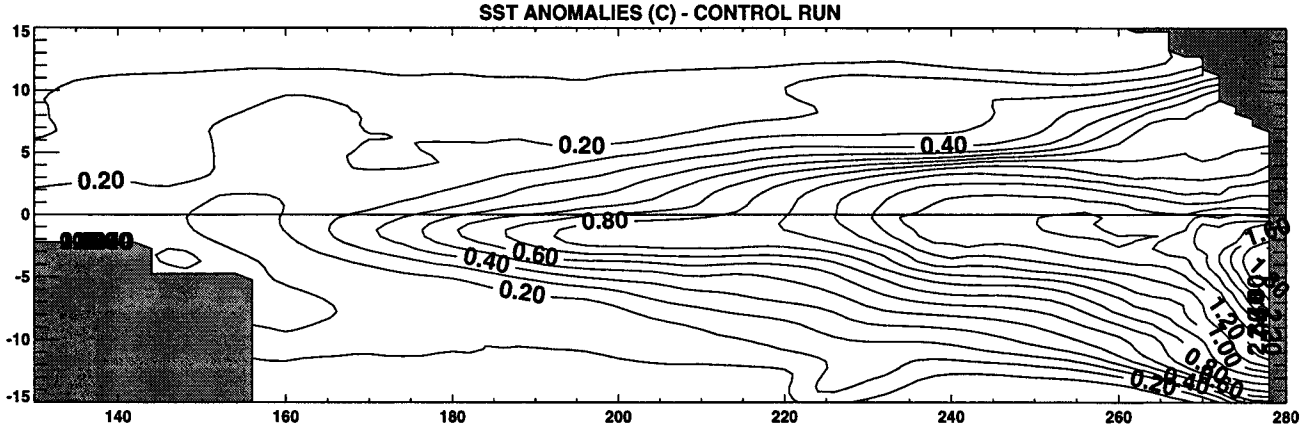

ZONAL PSEUDO-WIND STRESS ANOMALIES (DYN/CM2) - CONTROL RUN

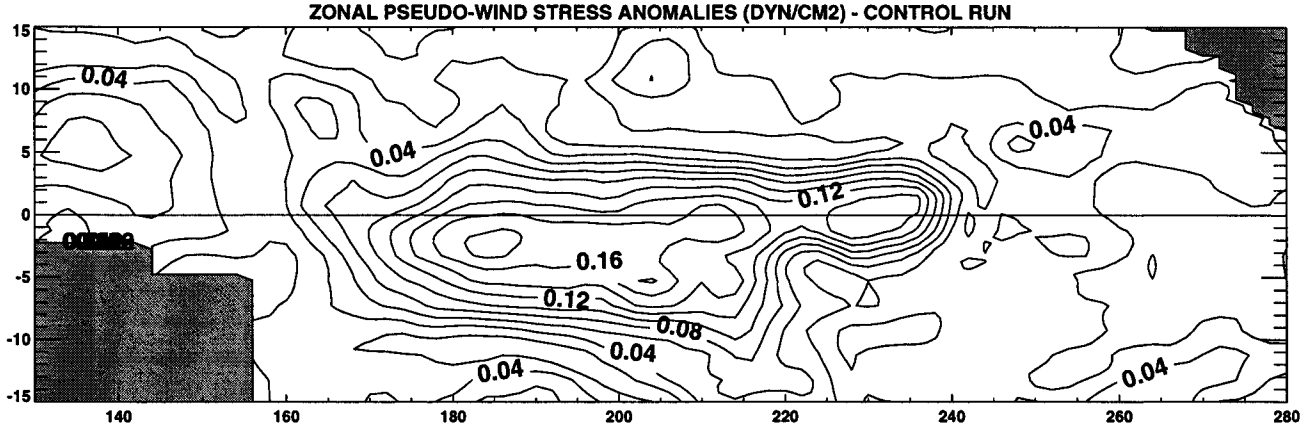

MERIDIONAL PSEUDO-WIND STRESS ANOMALIES (DYN/CM2) - CONTROL RUN

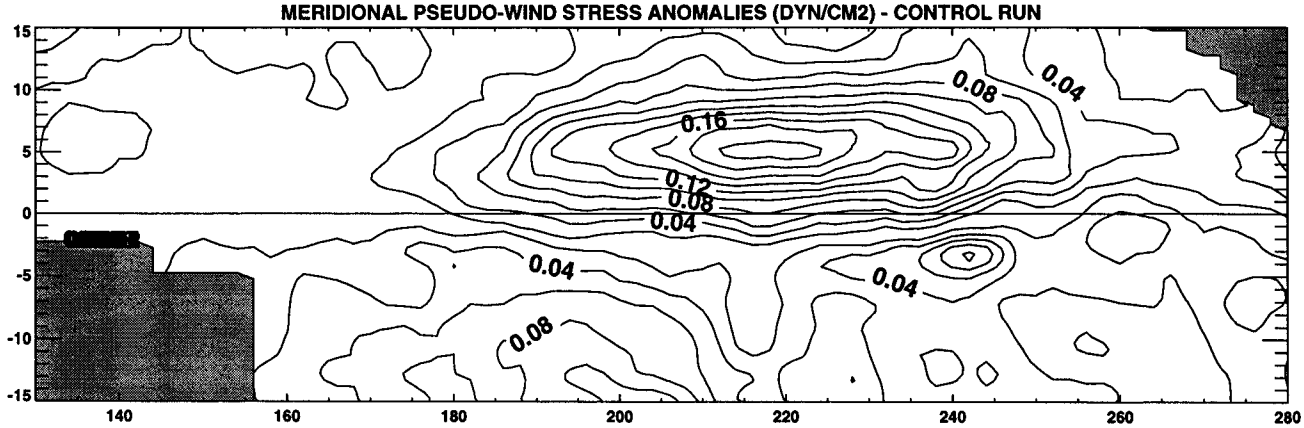

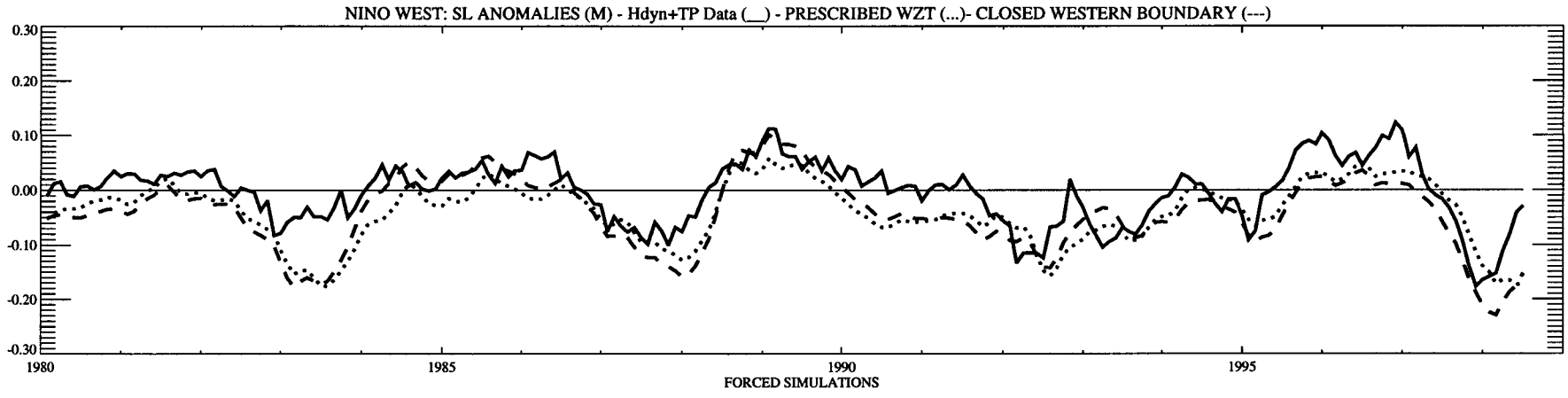
NINO WEST: SL ANOMALIES (M) - Hdyn+TP Data (__) - PRESCRIBED WZT (...)- CLOSED WESTERN BOUNDARY (---)
0.30
0.20
0.10
0.00
-0.10
-0.20
-0.30
1980
1985
1990
1995
FORCED SIMULATIONS

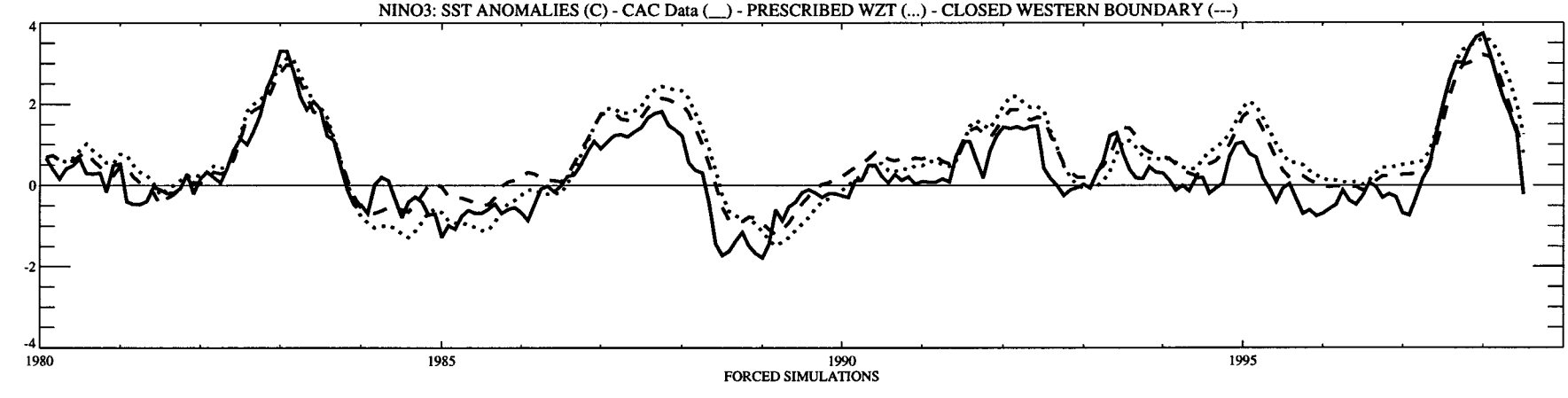
NINO3: SST ANOMALIES (C) - CAC Data (__) - PRESCRIBED WZT (...) - CLOSED WESTERN BOUNDARY (---)
4
2
0
-2
-4
1980
1985
1990
1995
FORCED SIMULATIONS

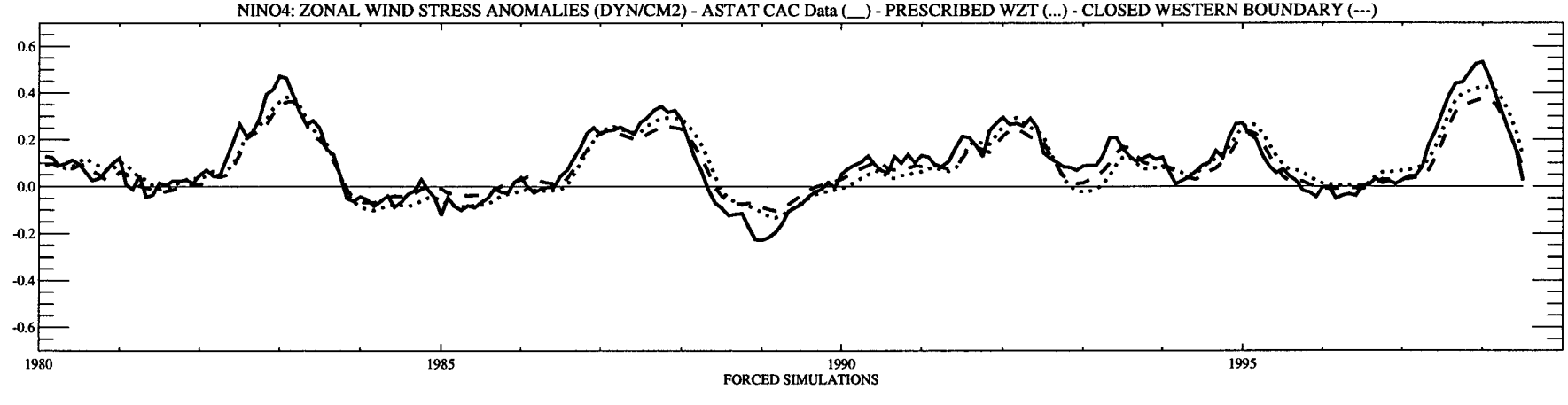
NINO4: ZONAL WIND STRESS ANOMALIES (DYN/CM2) - ASTAT CAC Data (__) - PRESCRIBED WZT (...) - CLOSED WESTERN BOUNDARY (---)
0.6
0.4
0.2
0.0
-0.2
-0.4
-0.6
1980
1985
1990
1995
FORCED SIMULATIONS

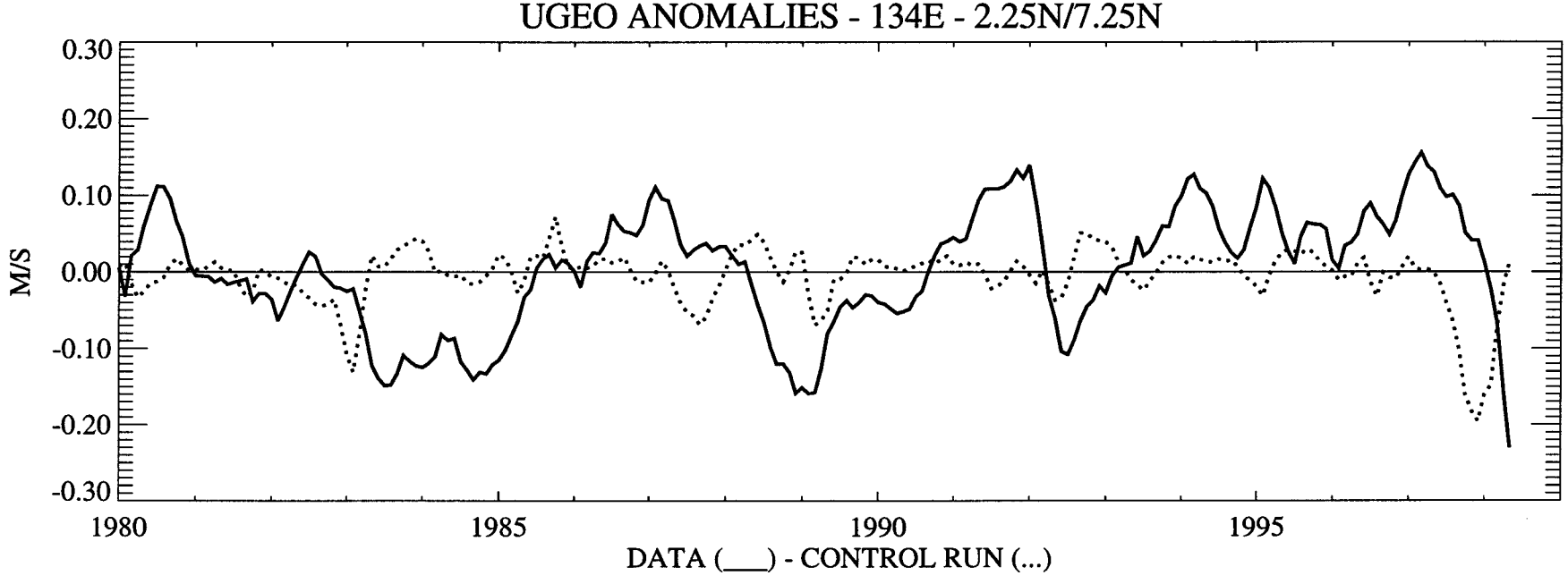
UGEO ANOMALIES - 134E - 2.25N/7.25N
0.30
0.20
0.10
0.00
-0.10
-0.20
-0.30
M/S
1980
1985
1990
1995
DATA (___) - CONTROL RUN (...)

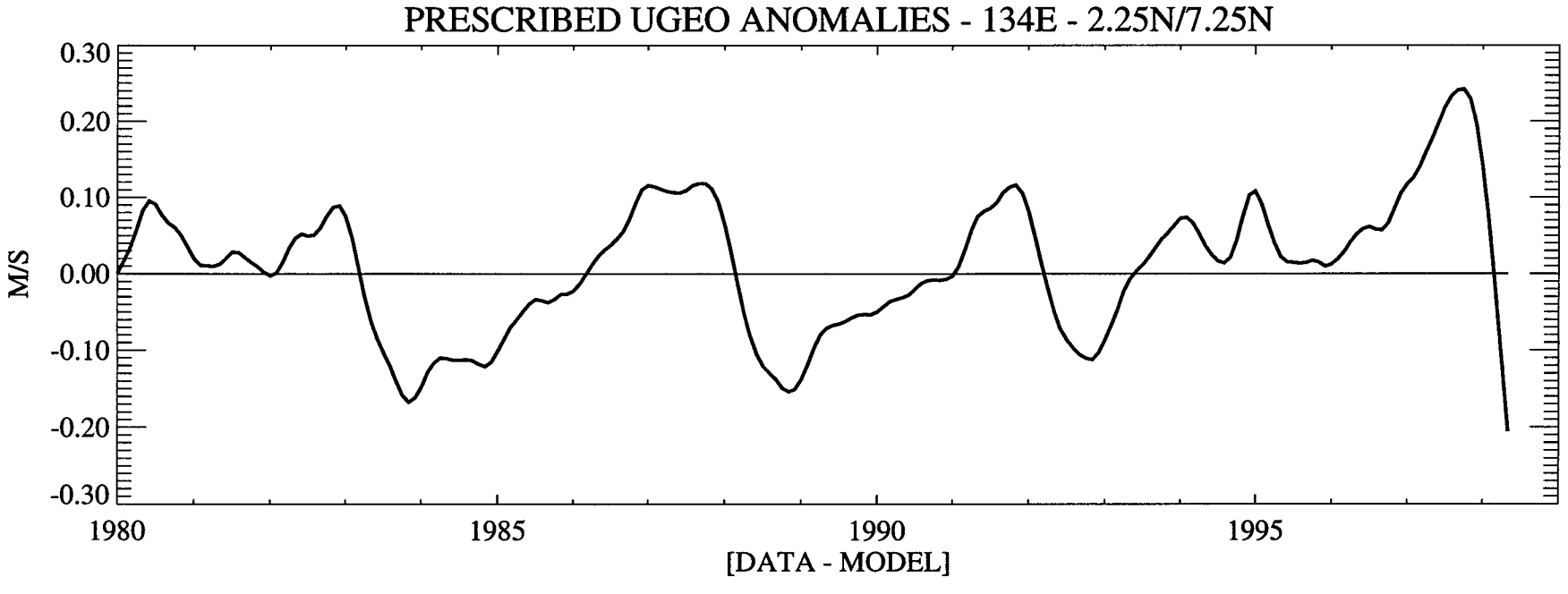
PRESCRIBED UGEO ANOMALIES - 134E - 2.25N/7.25N
0.30
0.20
0.10
0.00
-0.10
-0.20
-0.30
M/S
1980
1985
1990
1995
[DATA - MODEL]

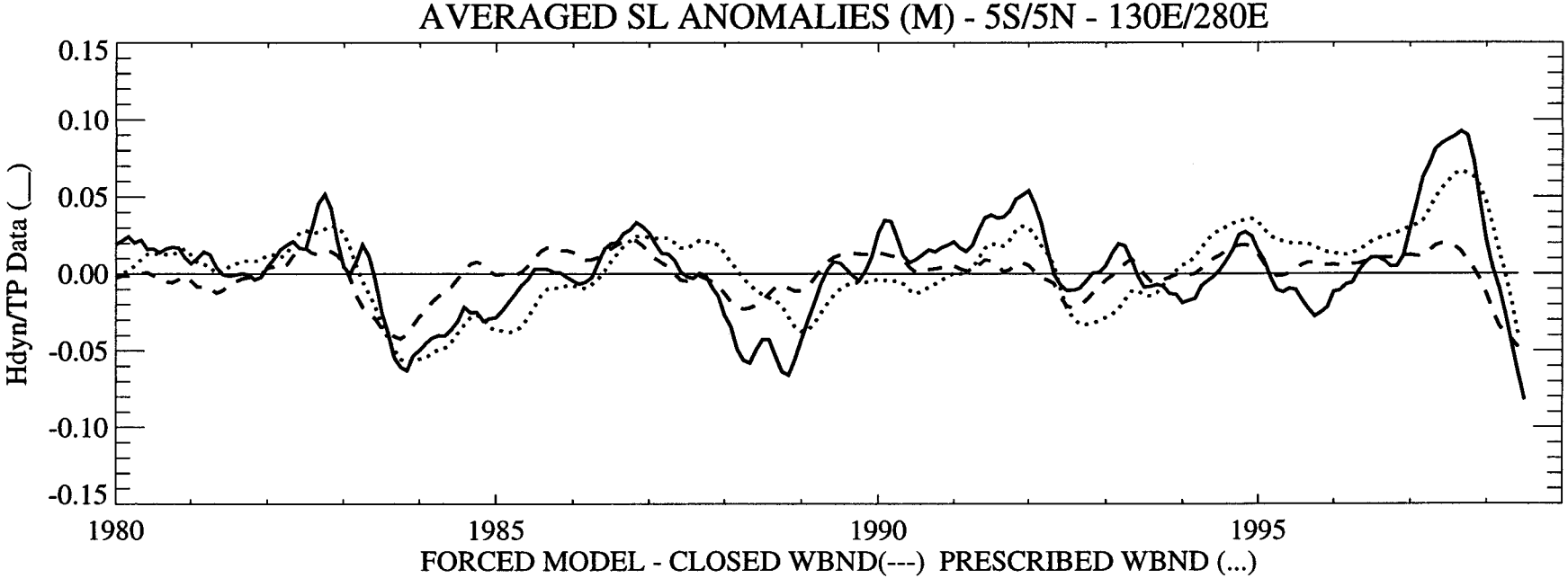
AVERAGED SL ANOMALIES (M) - 5S/5N - 130E/280E
0.15
0.10
0.05
0.00
-0.05
-0.10
-0.15
Hdyn/TP Data (_)
1980
1985
1990
1995
FORCED MODEL - CLOSED WBND(---) PRESCRIBED WBND (...)

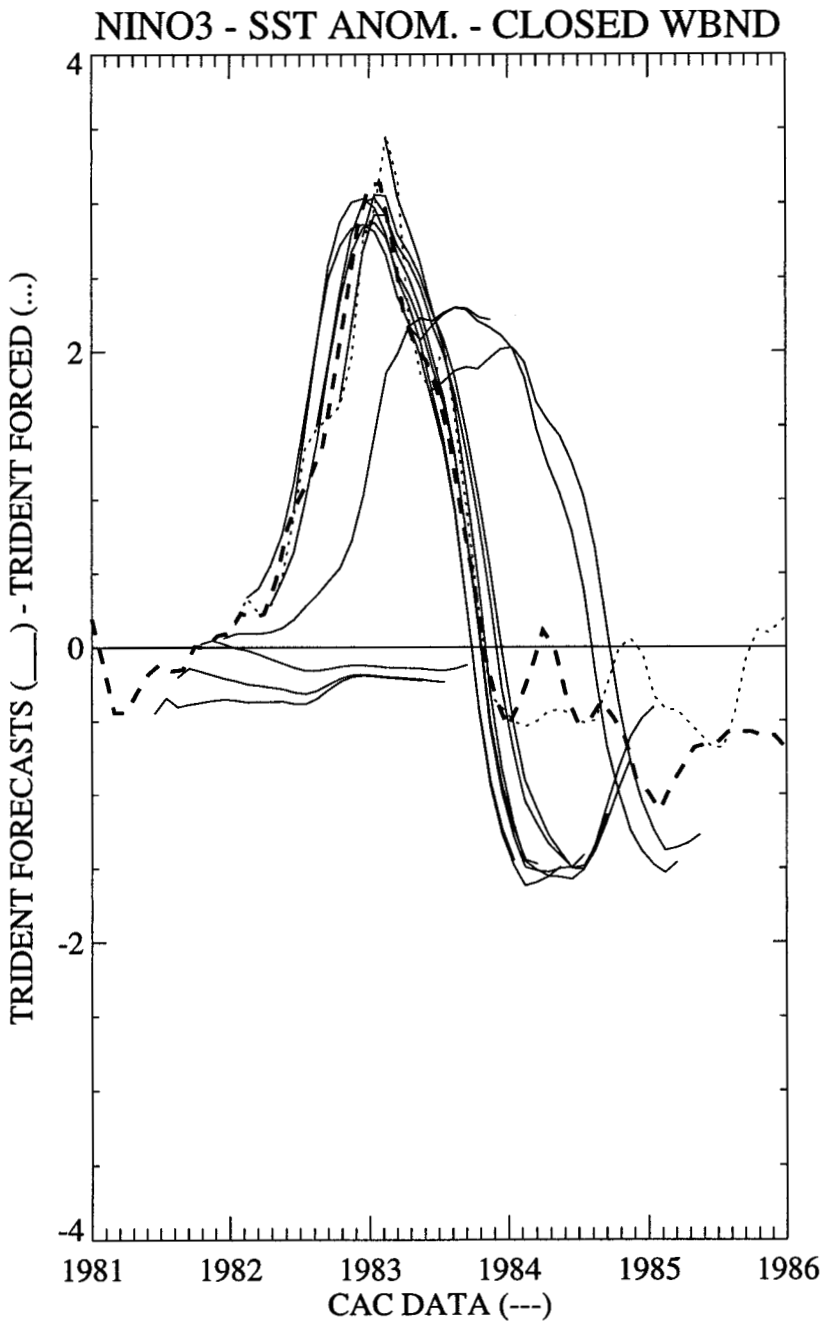
NINO3 - SST ANOM. - CLOSED WBND
TRIDENT FORECASTS (___) - TRIDENT FORCED (...)
4
2
0
-2
-4
1981
1982
1983
1984
1985
1986
CAC DATA (---)

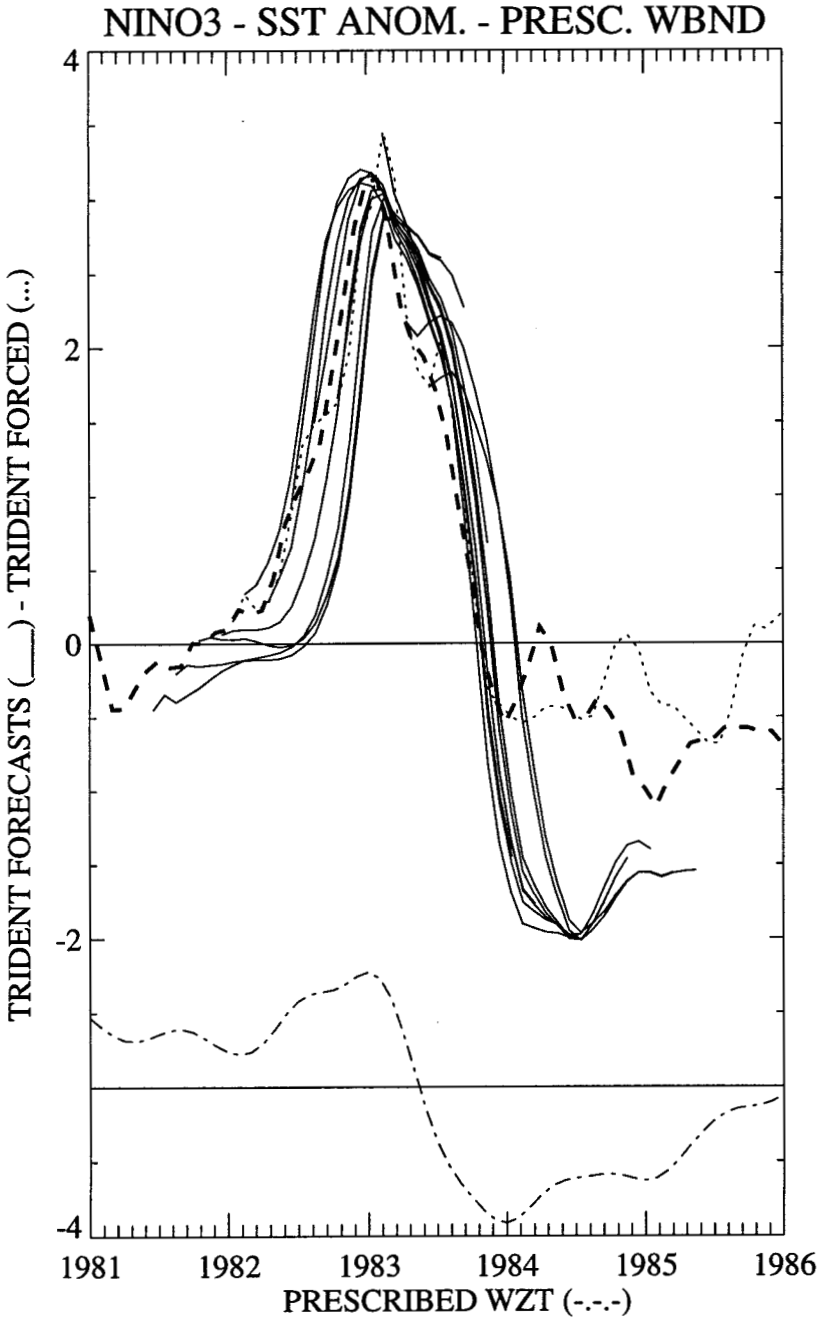
NINO3 - SST ANOM. - PRESC. WBND
TRIDENT FORECASTS (___) - TRIDENT FORCED (...)
4
2
0
-2
-4
1981
1982
1983
1984
1985
1986
PRESCRIBED WZT (-.-.-)